Improving Material Identification Capabilities in Neutron Tomography via Monte Carlo Simulations and Artificial Neural Networks

Christopher S. Cogliano and Zeyun Wu

Department of Mechanical and Nuclear Engineering, Virginia Commonwealth University, Richmond, VA, 23284
coglianoc@vcu.edu; zwu@vcu.edu

INTRODUCTION

Neutron tomography (NT) is a powerful non-destructive technique used to infer the internal material structure of a target object by analyzing emitted or transmitted neutron radiation, typically through multiple radiographic projections from different viewing angles [1]. This technique is uniquely capable of accurately distinguishing materials containing elements with lighter atomic nuclei, even if they are shielded by materials with heavier nuclei [1]. With advances in computational simulation technology and the rapid development of artificial intelligence (AI), significant new opportunities exist to further enhance NT image reconstruction techniques [1].

The objective of this study is to employ Monte Carlo simulations - specifically the Monte Carlo N-Particle Transport (MCNP) code - to develop a realistic neutron radiography imaging platform for a target object. Extensive measurement datasets are generated through multiple simulation trials with varying material composition. Building upon these results, an artificial neural network (ANN) will be developed to identify materials within unknown objects based on their radiographic signatures, with training, validation, and testing datasets derived from the MCNP simulations. The results of this project have the potential to enable novel applications in nuclear safeguards and security, analysis of automotive and aerospace components, and medical imaging [2].

METHODOLOGY

Background and Theory

Developed by Los Alamos National Laboratory, MCNP is a general-purpose, continuous-energy, generalized-geometry, and time-dependent Monte Carlo radiation transport code designed to track many particle types over a broad range of energies [3]. Fundamentally, a Monte Carlo simulation theoretically duplicates a random walk process, which governs the interactions between nuclear particles and materials [3]. For example, Fig. 1 represents the random history of a neutron incident on a slab of fissile material. This method is particularly useful for complex problems that computer codes that use deterministic methods struggle to model accurately and/or efficiently [3].

To perform particle tracking, the MCNP code provides various standard tally types that can be specified by the user and are automatically normalized to be per source particle. One of these tally types can be used as a point detector, which is a deterministic estimate (from the current event point) of the neutron flux at a point in space [3]. Contributions to the point detector tally are made at source and collision events throughout the random walk [3]. The physical quantity described by the point detector neutron flux tally is shown using the following expression below in Eq. (1)

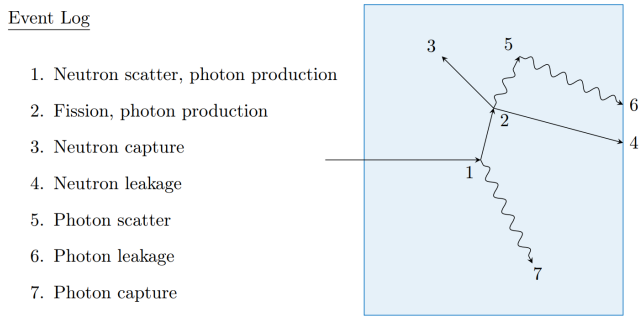

Fig. 1. Various particle random walks. The zigzag lines represent photon movement, however the MCNP code treats the moving of photons as straight lines between collisions. Image retrieved from [3].

$$\phi_P = \int dE \int dt \int d\Omega \psi(\boldsymbol{r}_P, \boldsymbol{\Omega}, E, t), \tag{1}$$

where ϕ_P is the neutron flux at a point, ψ is the angular flux as usually defined in nuclear reactor theory, and $\boldsymbol{r}_P, \boldsymbol{\Omega}, E, t$ are the neutron position vector (cm), direction unit vector, energy (MeV), and time (shakes, sh; 1 sh = 10^{-8} s), respectively [3]. The units for the point neutron flux physical quantity are particles/cm^2.

To accurately estimate the physical quantity described in Eq. (1), each neutron tally quantity is scored in the MCNP code before final normalization using the expression shown below in Eq. (2)

$$S_n = \frac{W \cdot p(\boldsymbol{\Omega}_P) \exp(-\lambda)}{L^2}, \tag{2}$$

where S_n is the score (pre-normalization) for the neutron count tally quantity, W is the particle weight, $p(\boldsymbol{\Omega}_P)$ is the probability density function for scattering (or starting) in the direction $\boldsymbol{\Omega}_P$ towards the point detector assuming azimuthal symmetry, λ is the total number of free mean paths from the particle location to the detector (i.e the optical distance), and L is the distance to the detector from the source or collision event (cm) [3]. The units for the point neutron detector flux tally score are also particles/cm^2.

Additionally, this tally can be modified to change the units into energy flux, thus the neutron tally quantity is scored in the MCNP code before final normalization as shown below in Eq. (3)

$$S_E = \frac{W \cdot p(\boldsymbol{\Omega}_P) \exp(-\lambda) E}{L^2}, \tag{3}$$

where S_E is the score (pre-normalization) for the neutron energy tally quantity, W, $p(\mathbf{\Omega}_P)$, λ, and L are the same parameters from Eq. (2), and E (MeV/cm^2) is the neutron energy [3]. The units for the point neutron detector energy flux tally score are MeV/cm^2.

In order for MCNP to mimic neutron imaging, it uses flux image detectors, which are an array of point detectors that are close enough to each other to generate an image based on their respective neutron or energy fluxes [3]. Here, each detector point represents one pixel of the neutron or energy flux image. For this study, both multiple neutron and energy Flux Image Radiograph (FIR) tallies are used, which act like film for an x-ray type of image (in essence, a transmitted image but with neutrons instead of photons used in traditional x-rays) [3]. Fig. 2 shows how the FIR planar rectangular grid image is defined for a source particle scattering and passing through a target object.

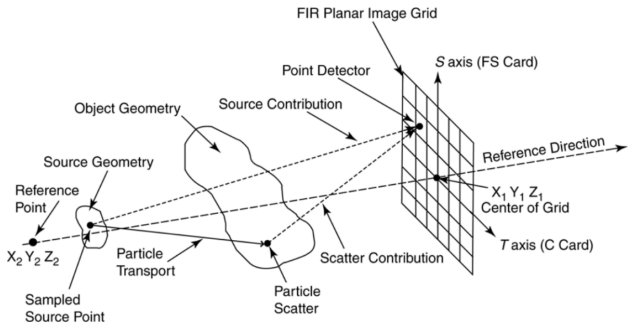

Fig. 2. Diagram of an FIR tally for a source external to the object. The directions of the orthogonal S- and T-axes depend on the reference-direction vector in the geometry coordinate system. Image retrieved from [3].

Problem Configuration

For this study, an MCNP model that resembles a realistic energy range for a NT experiment was initially constructed. In general practice, a ^{252}Cf spontaneous fission (SF) source is used to generate fast neutrons for non-destructive imaging capabilities. Thus, this model's source samples neutron energies from the Watt fission spectrum, with its parameters corresponding to ^{252}Cf SF as shown in Eq. (4) below

$$p(E) = C\exp(-E/a)\sinh(\sqrt{bE}), \tag{4}$$

where $p(E)$ is the energy sampling probability function, C = 0.63802 (normalization constant), E is the sampled energy value (MeV), a = 1.18 MeV (^{252}Cf SF parameter), and b = 1.0342 MeV^{-1} (^{252}Cf SF parameter) [4].

To optimize computational efficiency during MCNP model development, the neutron source in the code was designed to resemble an ideal collimator, where all neutrons are set to move in the same direction directly towards the target object. Thus, the neutron source in this initial model is a unidirectional beam normal to the circular surface (r = 3 cm) it originates from and the front FIR tally planes.

The target object in this model is a cylinder (r = 2 cm, h = 2 cm) with its center 5 cm ahead of the center of the neutron source in the direction of the neutron beam. In this initial MCNP model, there are two different simulation configurations that vary the orientation of the target object: *Configuration A* and *Configuration B*. In the *Configuration A* simulation, the cylinder is oriented such that its flat face is perpendicular to the source surface, whereas in the *Configuration B* simulation, the cylinder's flat face is parallel to the source surface. Besides the target object orientation, every simulation parameter between *Configuration A* and *Configuration B* remain the same.

The initial model contains three neutron and three energy FIR tally detector planes. There are three different locations for the FIR tallies, where each location contains a tally pair consisting of one neutron FIR detector plane and one energy FIR detector plane, both perfectly overlapping each other. The first location (the front) has detectors that are centered 5 cm ahead of the center of the target object in the direction of the neutron beam and oriented parallel to the source surface. The second location (the top) has detectors centered 5 cm above the center of the target object in the direction perpendicular to the neutron beam and is oriented perpendicular to the source surface. The third location (the bottom) is configured the same as the second location, except the detectors are centered 5 cm below the center of the target object instead of 5 cm above. Each detector plane is a square (s = 10 cm) where each side is divided into 50 tally bins, resulting in each FIR detector being able to produce a 2,500 pixel image. Additionally, each FIR detector tally also has energy bins that are split into three different sections: thermal (0 – 0.5 eV), intermediate (0.5 eV – 0.5 MeV), and fast (0.5 – 20 MeV). For only the energy FIR tallies, each of these three sections is equally divided into 20 different energy bins. Fig. 3 and Fig. 4 show the initial MCNP model geometry setups for *Configuration A* and *Configuration B*, respectively, with both models displaying the three overlapping neutron and energy FIR tally pairs, the cylindrical target object, and the unidirectional neutron source with all values on the axes in cm.

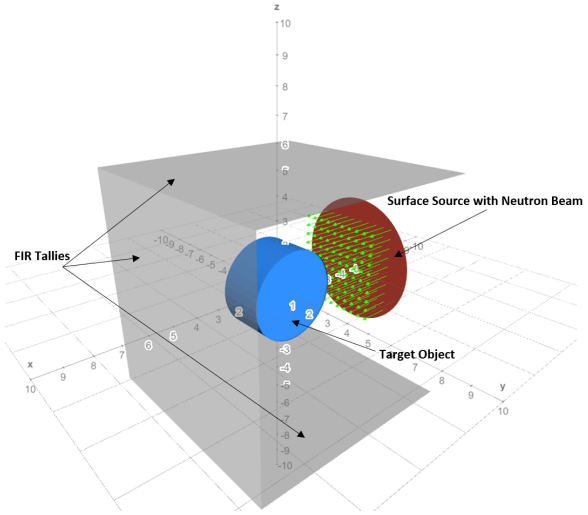

Fig. 3. Diagram of the initial MCNP model geometry for *Configuration A*

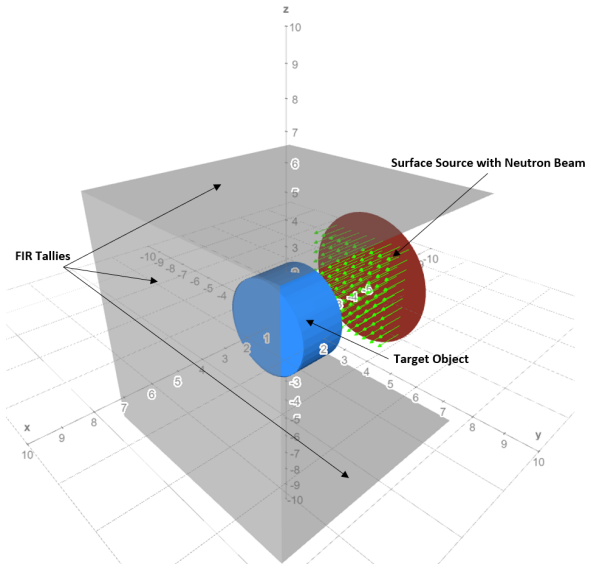

Fig. 4. Diagram of the initial MCNP model geometry for *Configuration B*

Data Library for Material Identification

In this study, multiple MCNP simulations will be performed using a single baseline model, with each simulation varying only the material composition of the target object while all other parameters are held constant. To effectively train, validate, and test the ANN model developed later, a comprehensive dataset will be generated from a curated selection of materials spanning diverse application domains, including nuclear reactor and fuel-related materials, adhesives and sealants, and energetic materials. These materials are selected to encompass a wide range of elemental compositions and neutron interaction characteristics. For each material, simulations will be conducted using the established MCNP model, and extensive data will be collected from the FIR tallies and stored in a structured data library. Thus, with subsequent integration of this library into the ANN framework, the ANN will be able to recognize and identify the material composition of an unknown object by examining its neutron imaging data.

RESULTS

During the MCNP model development phase of this study, each iteration was evaluated through a series of simulations in which key parameters - such as particle count, FIR image resolution, and material composition - were systematically varied. In particular, light water was used as a reference test material for all model iterations due to its strong moderating effect on fast neutrons. The preliminary results presented here are the most recent iteration of the MCNP model developed in the study.

Neutron Imaging of Light Water Cylinder

Following execution of the most recent MCNP model with the target object composed of water, both quantitative and qualitative results were produced.

The MCNP model output displayed data corresponding to each pixel, which compose the images generated by each neutron and energy FIR tally detector in both the *Configuration A* and *Configuration B* simulations. Specifically, for the neutron FIR tallies, this pixel data lists the pixel's position on the tally plane and the normalized neutron flux values with their corresponding relative errors both divided by energy range (thermal, intermediate, and fast) and in total including all energies $0-20$ MeV. As for the energy FIR tallies, the pixel data is formatted the same as the neutron FIR tallies, except that it lists normalized neutron energy flux values instead of neutron flux values.

Each pixel is assigned a color based on the magnitude of its total normalized neutron flux or normalized neutron energy flux relative to other pixels in the FIR detector plane. When all 2,500 pixels are combined, a complete radiographic image is formed. Fig. 5 shows an image produced by the front neutron FIR tally detector with a relative error of 0.42%, incorporating contributions from all neutron energy bins for the *Configuration A* simulation. The values on both the vertical and horizontal coordinate axes range from -10 to 10 centimeters.

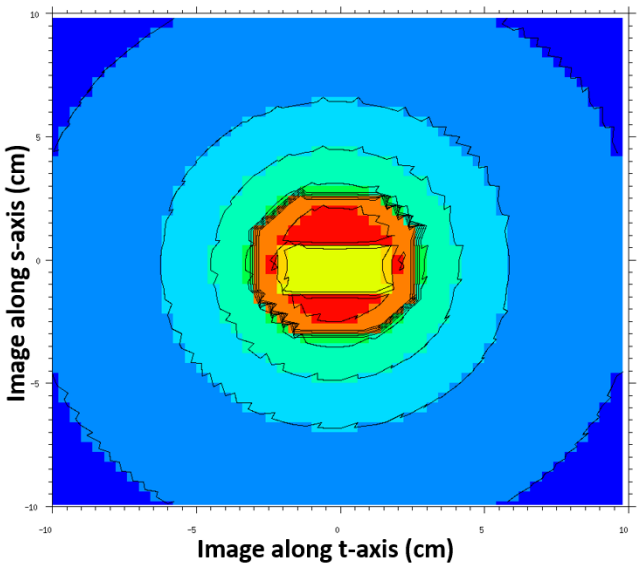

Fig. 5. Two-dimensional image of light water cylinder produced by front neutron FIR tally in *Configuration A*

The bottom and top tallies are positioned so that they do not intersect the neutron beam. Consequently, all recorded flux in these tallies originates from scattered neutrons. For example, Fig. 6 presents an image generated by the top energy FIR tally detector with a relative error of 0.42%, incorporating contributions from all neutron energy bins for the *Configuration B* simulation. The values on the vertical and horizontal coordinate axes values are exactly the same as those from Fig. 5. Fig. 7 displays a zoomed-in image of the normalized neutron and energy flux values corresponding to each pixel color from the images produced by the front neutron (Fig. 5) and the top energy (Fig. 6) FIR tally detectors.

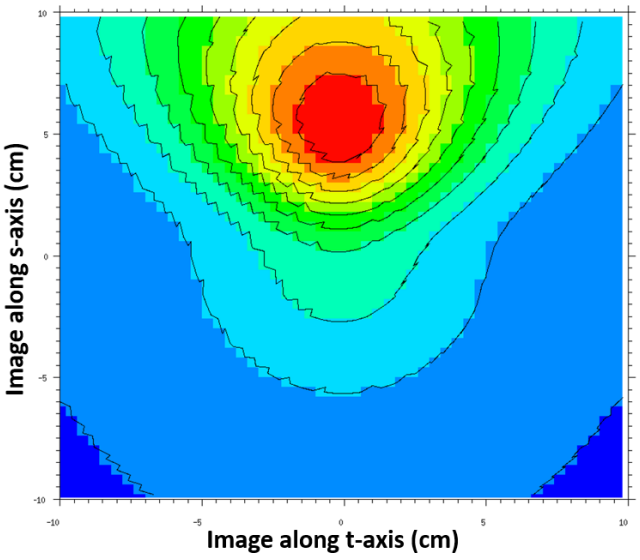

Fig. 6. Two-dimensional image of light water cylinder produced by top neutron energy FIR tally in *Configuration B*

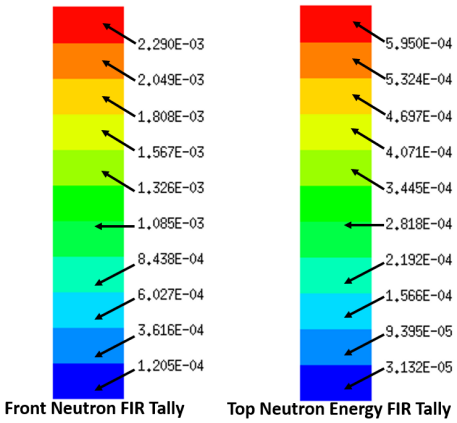

Fig. 7. Legends for images produced by front neutron and top neutron energy FIR tallies showing normalized neutron flux (left) and normalized neutron energy flux (right) values corresponding to each displayed color

These results indicate that water strongly interacts with neutrons emitted from the ^{252}Cf SF, as attenuation, moderation, and scattering in the light water produces a distinct projection in the FIR tally images.

FUTURE WORK

Further MCNP Model Developments

Several enhancements are planned to further improve the realism of the MCNP model. For example, a compact micro-collimator incorporating microchannel plates (MCPs) will be added to attenuate neutrons that are not incident normal to the front detector plane, thereby producing an effectively unidirectional neutron beam downstream of the collimator [5]. With the inclusion of this collimator, the neutron source model will be revised from a unidirectional surface source to an isotropic point source.

In addition, a series of target object orientation configurations will be introduced, in which the cylinder object in *Configuration A* is incrementally rotated until it reaches the orientation used in *Configuration B*. The rotation will be defined by a fixed angular increment, $\Delta\theta$, such that each simulation corresponds to a successive rotation step, θ_i. This approach will enable the combination of radiographic images from multiple orientations to reconstruct three-dimensional neutron tomographic images. Prior to collecting the full simulation dataset, the MCNP model will be validated by comparing its results against relevant published literature.

ANN Developments

Following completion of data collection using the MCNP model, the next phase of the study will focus on developing a convolutional neural network (CNN) trained, validated, and tested using the simulated radiographic datasets. CNNs are well suited for analyzing grid-structured data, such as images, as they employ convolutional and pooling layers to extract hierarchical spatial features, including edges, shapes, and textures [6]. Accordingly, this architecture is well suited for inverse transport analysis, in which the network analyzes the characteristics of emergent neutron radiation to infer the material composition of the interrogated object [6].

The CNN will be implemented using Keras, a high-level Python-based application programming interface integrated with TensorFlow, which provides the underlying machine learning framework and supports scalable deployment [6]. Keras is designed to streamline the development, training, and deployment of ANNs [6].

ACKNOWLEDGMENTS

This work is supported by the Enabling Technologies & Innovation 2.0 Consortium under the U.S. National Nuclear Security Administration Office of Defense & Nuclear Nonproliferation's Research & Development program.

REFERENCES

1. J. YANG, "Deep learning methods for neutron image restoration," Tech. rep., Northeast Normal University (2023).
2. B. JOSEPH, "A systematic review on neutron radiography: applications, advantages, and challenges," Tech. rep., Ramaiah University of Applied Sciences (2025).
3. Los Alamos National Laboratory, *MCNP Code Version 6.3.0 Theory & User Manual*, 2nd ed. (2022).
4. F. FROEHNER, "Watt spectrum fit to 252Cf prompt fission neutron data," Tech. rep., International Atomic Energy Agency (1988).
5. B. JOLICOEUR, "Development of a Micro Collimator Array for Neutron Radiography," Tech. rep., Worcester Polytechnic Institute (2022).
6. F. CHOLLET, *Deep Learning with Python*, Manning Publications Co., 2nd ed. (2021).